

Impact of ICRH on the Measurement of Fast Ions by Collective Thomson Scattering in ITER

M. Salewski 1), L.-G. Eriksson 2), H. Bindslev 1), S. B. Korsholm 1), F. Leipold 1), F. Meo 1), P.K. Michelsen 1), and S. K. Nielsen 1)

1) Association Euratom - Risø DTU, Risø National Laboratory for Sustainable Energy, Technical University of Denmark, DK-4000 Roskilde, Denmark

2) Association Euratom - CEA, CEA/DSM/DRFC, CEA-Cadarache, F-13108 St. Paul lez Durance, France

e-mail contact of main author: mirko.salewski@risoe.dk

Abstract. Collective Thomson scattering (CTS) has been proposed for measuring the phase space distribution of confined fast ion populations in ITER plasmas. This study determines the impact of fast ions accelerated by ion cyclotron resonance heating (ICRH) on the ability of CTS to diagnose fusion alphas in ITER. The investigated ICRH scenarios include pure second harmonic tritium heating and ^3He minority heating at a frequency of 50 MHz, corresponding to an off-axis resonance. The sensitivities of the results to the ^3He concentration (0.1–4%) and the heating power (20–40 MW) are considered. Fusion born alphas dominate the total CTS signal for large Doppler shifts of the scattered radiation. The tritons generate a negligible fraction of the total fast ion CTS signal in any of these heating scenarios. The minority species ^3He , however, contributes more than 10% of the fast ion CTS signal at locations close to the resonance layer for ^3He concentrations larger than $\sim 1\%$. In this particular region in space for resolution of near perpendicular velocities, it may be difficult to draw conclusions about physics of alpha particles alone by CTS. With this exception, the CTS diagnostic can reveal the physics of the fusion alphas in ITER even under presence of fast ions due to ICRH.

1. Introduction

Fast ions in present plasma confinement devices are mainly produced by auxiliary heating methods: Ion cyclotron resonance heating (ICRH) and neutral beam injection (NBI). In ITER, however, the dominant source of fast ions and heating will be the deuterium – tritium fusion reaction producing energetic alpha particles [1, 2]. These fast ions with energies up to several MeV need to be well confined while they slow down as the fast ion confinement has direct impacts on the achievable heating efficiency. Additionally, the losses of energetic ions to the wall need to be limited to avoid unacceptable heat loads on the wall, especially in view of the very long pulse times and large energetic ion populations planned for ITER [3]. In burning plasmas, therefore, fast ions play an even more important role than in current plasmas.

Fast ion losses due to single-particle effects are relatively well understood, but fast ion losses due to collective behaviour are much more challenging. Among these are the normal modes such as the family of Alfvén gap modes, kinetic ballooning modes, and internal kink modes [4, 5]. Perhaps the most serious of these in ITER is the toroidal Alfvén eigenmode [6–10]. Also of importance in a burning plasma may be the branch of energetic particle modes [11, 12]. These classes of modes may redistribute and eject fast ions, and their interaction with the less anisotropic fast ion populations of burning plasmas with a higher degree of self-organization is still not accurately known. It has also been suggested that electrostatic turbulence may enhance fast ion transport [13]. The radial transport of fast ions may be large due to these effects.

The measurement of phase space distributions of confined fast ions is all the more important for understanding these energetic ion physics issues in the burning plasma regime. Measurement of fast ions in ITER is essential for benchmarking the predictions made by current theories. Collective Thomson scattering (CTS) is a multi-faceted diagnostic with which the 1D fast ion velocity distribution function in plasmas can be determined. This has been demonstrated at JET and TEXTOR [14–17].

ICRH accelerates ions to large velocities perpendicular to the magnetic field, leading to strongly anisotropic fast ion distributions. In burning plasmas, there is additionally the approximately isotropic population of fusion alphas. The fast ions due to ICRH may affect the CTS alpha measurements near the perpendicular direction (see section 2): It is not feasible to tell from the measured CTS signal how large the contributions of the various fast ion species to the measured signal are. For example, an alpha produces as much CTS signal as four tritons moving at the same velocity. Nevertheless, their fractions of the total CTS signal can be found by modeling [18, 19]. This is performed here in a series of synthetic diagnostic experiments with the goal to determine which species will dominate the signal for the planned ITER CTS diagnostic resolving near perpendicular velocities and will therefore be amenable to direct observation to a good approximation.

In previous studies, it could be concluded that NBI heating will not significantly affect the measurement of alpha particles in ITER [20, 21]. The present study focuses on ICRH and thereby complements the previous studies of NBI heating. The distribution functions for resonant tritons and ^3He (if present) have been computed with the PION code [22, 23] and the resulting contributions to the CTS signal with a fully electromagnetic model of CTS [18,19]. The assumed heating scenarios were pure tritium heating at the second harmonic resonance and ^3He minority heating at the fundamental resonance with ^3He concentrations from 0.1% to 4%. The ICRH frequency was set to 50 MHz, corresponding to an off-axis resonance on the low field side. The heating power was varied from 20 to 40 MW.

In section 2, the ITER CTS system and the models describing it are discussed. Modeling of the plasma parameters, among these the fast ion distributions, is described in section 3. Section 4 contains the computed fast ion distributions and corresponding CTS spectra for resolution of near perpendicular velocities in the heating scenarios mentioned above, and conclusions are drawn in section 5. The results indicate that the CTS signal in the frequency bands of interest will mostly originate from fusion born alpha particles. Fast tritons produce a negligible fraction of the CTS signal compared to fusion alphas in any investigated heating scenario. However, if the minority species ^3He is present in concentrations larger than 1%, it generates a significant fraction of the CTS signal (>10%) in the outer frequency bands typical for fast ions at locations close to the resonance layer.

2. Collective Thomson Scattering Modelling and Design for ITER

Microscopic fluctuations in the plasma will scatter radiation from a beam of radiation passing through the plasma. The ion velocity distribution can be inferred from the microscopic fluctuations with a wavelength larger than the Debye length λ_D , i.e. $k^\delta \lambda_D < 1$, where k^δ is the magnitude of the fluctuation wave vector \mathbf{k}^δ . In the experiment, a beam of probing radiation with wavenumber \mathbf{k}^i is launched into the plasma, and part of the scattered radiation with wavenumber \mathbf{k}^s is detected by a receiver. The measurement is spatially localized in the so-called scattering volume which is given by the overlap of probe and receiver beams. The receiver beam is an imagined beam which would emerge if one followed the path of radiation accepted by the receiver in reverse direction. Example probe and receiver beams and a scattering volume in ITER are sketched in Figure 1. The wavenumbers and frequencies (with

identical superscripts) are related by the matching conditions $(\mathbf{k}^\delta, \omega^\delta) = (\mathbf{k}^s - \mathbf{k}^i, \omega^s - \omega^i)$. The fluctuation frequency ω^δ driven by a fast ion can be approximately related to the ion velocity by $\omega^\delta = \mathbf{v}_{\text{ion}} \cdot \mathbf{k}^\delta$. This corresponds to resolution of the projection of the full velocity distribution function along the direction of \mathbf{k}^δ in the scattering volume. The measurable quantity in CTS is the spectral power density of scattered radiation which is proportional to the scattering function Σ . The scattering function accounts for the spectral variation in the scattered radiation due to microscopic fluctuations in the plasma. It is considered in a fully electromagnetic model and depends on fluctuations in electron density, the electric field, the magnetic field, and the current [18, 19]. We present the results in this study in terms of the scattering function.

The proposed ITER CTS system is designed to measure time-resolved fast ion velocity distributions in several measurement volumes simultaneously, satisfying the ITER measurement requirements for fusion alpha diagnostic [24]. It is divided into two subsystems, one for measuring fast ion velocity distributions in near perpendicular directions and one for near parallel directions [25-27]. The subsystem we focus on here has a launcher, which couples electromagnetic radiation at 60 GHz with 1 MW power in X mode into the plasma, and a receiver antenna on the low field side (LFS). This geometry permits resolution of near perpendicular velocities and is therefore relevant for the measurement of fast ions accelerated by ICRH. The CTS subsystem for resolution of near perpendicular velocities is sketched in Figure 1(a). The location of the scattering volume is described here by coordinates R (distance from the torus center) and Z (height above the plane which contains the magnetic axis). Two angles are most relevant when describing the scattering geometry: The angle Φ between the magnetic field vector \mathbf{B} and \mathbf{k}^δ and the scattering angle θ between the probe and receiver beams.

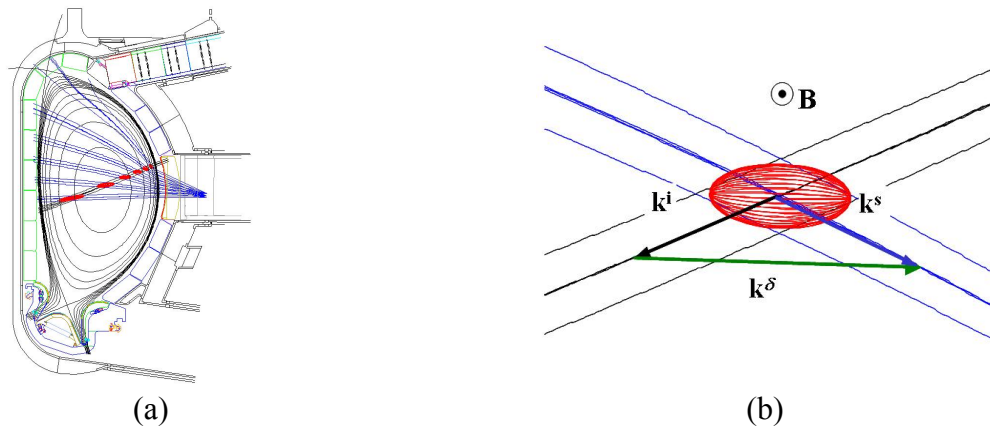


FIG. 1. Sketch of the CTS subsystem for ITER showing resolution near perpendicular to the magnetic field; (a) ITER poloidal plane with a probe and several receiver beams; (b) Scattering geometry with scattering volume as overlap of probe and receiver beams

3. Modelling of Plasma Parameters

The profiles of the bulk ion species, impurities, and the electrons at the respective measurement location are assumed to be given by the steady-state ITER plasma equilibrium [28]. The parameters for this ITER scenario were taken from simulations with the ASTRA code [29]. We assume bulk plasma species to have Maxwellian distribution functions and the

fusion alphas to have an isotropic classical slowing down distribution. The 4D distribution functions ($R, Z, v_{\parallel}, v_{\perp}$) of the fast ion populations from ICRH have been calculated with the PION code [22, 23]. In the simulations for the CTS diagnostic presented here, it is important to assess the pitch angle dependence of the distribution functions of the resonating ions. For this purpose the standard PION version has been upgraded with a module providing a model for the pitch angle distribution in the small banana width limit which is similar to that found in e.g. Ref. [30]. This model should provide acceptable results in cases for which finite orbit width effects are not expected to be important. It is important to note that the simulations presented here do not include self-consistent coupling between the plasma parameter profiles and the auxiliary heating. Additionally, information about the hardware details of the ICRH system is still not available. These uncertainties limit the conclusions that can be drawn.

4. Results

4.1 Second Harmonic Tritium Heating

The standard ITER reference design relies on second harmonic tritium heating with a power level of 20 MW. We vary additionally the ICRH power to 40 MW. For bulk ion heating, it is advantageous to move the cyclotron resonance somewhat to the LFS [31]. The scenarios considered here therefore have the nominal magnetic field on axis, 5.3 T, and an ICRH frequency of 50 MHz, placing the second harmonic cyclotron resonance of tritons on the LFS. In this case, PION simulations suggest that finite orbit width effects only play a minor role.

Figure 2(a) provides an overview of the 2D velocity distribution function of tritium at $R = 6.85$ m and $Z = 0.77$ m for the scenario with 40 MW ICRH. This location of the scattering volume leads to the strongest triton CTS signal component compared to other locations. The energy distribution of tritium is plotted for various pitch angles together with a classical slowing down distribution for fusion alphas. The energy has been normalized by the atomic mass number such that the abscissa is proportional to the square of the ion speed. It is evident that the triton distributions are strongly anisotropic with large perpendicular velocities and small parallel velocities. Energy absorption in ICRH at the second harmonic increases with the Larmor radius, and tritons are hence accelerated to very high energies in the perpendicular direction. The population of resonating ions with large parallel velocities is so small that it is of no concern in the context of the present study, even in a scenario with 40 MW ICRH power. Therefore, the attention is focused on the near perpendicular velocities in this study, measurable with the scattering geometries presented in Figure 1.

Resonating ions from ICRH can typically be found in a rather narrow region. In this work, the configuration space is scanned in small steps ($\sim 2-3$ cm) to find this region: The strongest CTS signal contribution from tritium is found at $R = 6.85$ m and $Z = 0.77$ m as mentioned above. The scattering function for this geometry is presented in Figure 2(b) for a power of 40 MW. The total signal for each frequency shift v^{δ} is the sum of the individual components. The fusion alphas dominate the spectrum for frequencies from $\sim \pm 1-4$ GHz, the outermost tips of the wings corresponding to alpha birth velocities (high frequency shift) and the proximal ends of the wings to alpha ash (low frequency shift). At even larger Doppler shifts, the electrons generate the only significant feature in the spectrum, and the bulk ion CTS signal towers over the other species at smaller Doppler shifts ($< \sim \pm 1$ GHz). The bulk ions contain deuterium, argon, and beryllium. The tritons are singled out from the bulk (also from the thermal part) due to their highly energetic tail.

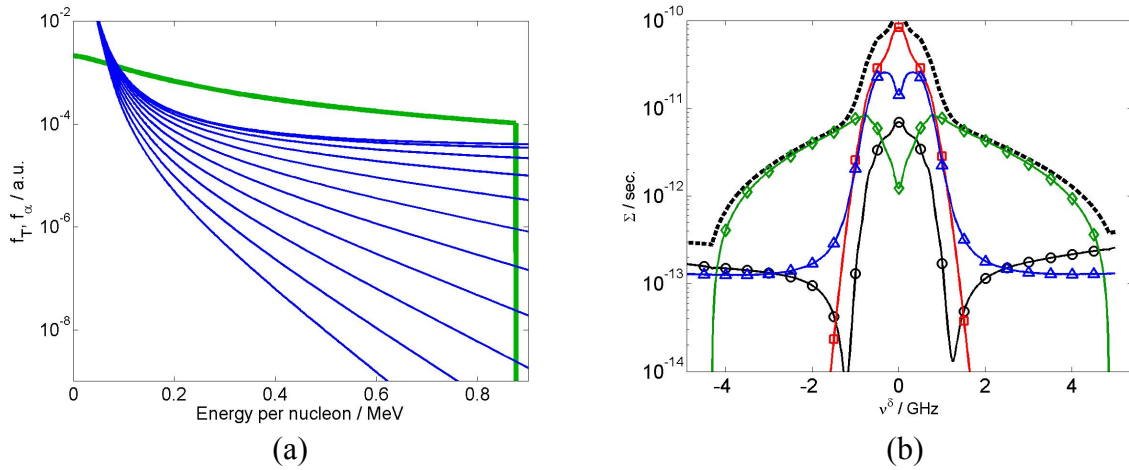


FIG. 2. Tritium distribution function and resulting CTS scattering function for pure second harmonic tritium heating with 40 MW ICRH power at $R = 6.85$ m and $Z = 0.77$ m; (a) Tritium distribution function compared to a classical slowing down distribution for alphas; green - alphas; blue - Tritium at various equally spaced pitch angles from 0° (bottom curve) to 90° (top curve); (b) Scattering function ($\Phi = 101^\circ$, $\theta = 156^\circ$); \blacklozenge -alphas, \blacktriangle -tritons, \blacksquare -bulk ions, \bullet - electrons, - - - total

Even for 40 MW ICRH power, twice the ICRH power currently planned for ITER, the contribution of the tritons to the total CTS signal with large Doppler shifts will be at least an order of magnitude below the alpha contribution and roughly level with the electron contribution. Part of the reason for the much weaker triton CTS signal component compared to the alpha component is that CTS signals are proportional to the square of the ion charge. Additionally, the volumetric heating rates are relatively moderate for second harmonic tritium heating as Figure 3(a) shows: The power deposition profiles are plotted as a function of the flux surface s . The power deposition profile on the tritium for second harmonic tritium heating may be compared to the power deposition profiles on ^3He for ^3He minority heating in Figure 5. The discussion of this comparison is deferred to section 4.2. The flux surface parameter is zero on the magnetic axis and one at the plasma edge. The ICRH power is mainly deposited between $s = 0.2$ and $s = 0.4$. The 40 MW scenario leads of course to a higher peak in the power deposition profile compared to the 20 MW scenario. In Figure 3(b), one representative frequency shift (+2.5 GHz) is plotted as a function of the major radius of the scattering volume for the reference power (20 MW) and the upgraded power (40 MW). The fusion alpha component is not affected by the two heating scenarios. If the ICRH power is increased, the triton CTS signal fraction will also increase as a result of the larger population of tritons at that frequency shift. The CTS signal component due to tritium in Figure 3(b) is strongest in a region with a width of about ~ 0.2 – 0.3 m located at a position around $R = 6.85$ m which was used for Figure 2. This width is comparable to the width of scattering volumes (~ 0.2 m). The spatial variation in the CTS signal component strength may be important due to this similarity in scale. In the modeling, a constant CTS signal throughout the scattering volume is assumed, leading to an overestimation at the maximum if the signal is non-uniform in configuration space (as for the clearly peaked tritium component). It should be noted that this does not hamper the conclusions which we draw. These considerations indicate that for ICRH of tritium at the second harmonic resonance (50 MHz), most of the fast ion CTS signal can be attributed to fusion alphas.

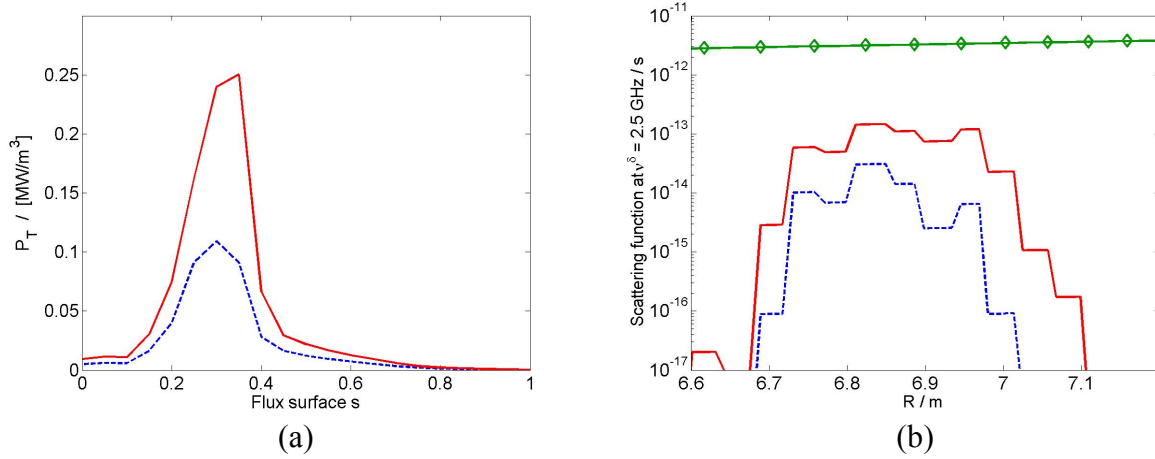


FIG. 3. Power deposition and scattering function profiles for pure second harmonic tritium heating; (a) Power deposition profile on tritons: — 40 MW, - - - 20 MW; (b) Scattering function at $\nu^\delta = 2.5$ GHz for various scattering volumes with different R; \blacklozenge - alphas, — tritons at 40 MW, - - - tritons at 20 MW

4.2 ^3He minority heating

^3He minority heating is an interesting option for ICRH since it increases the amount of power coupled into the ions rather than the electrons. Minority heating does not depend strongly on finite Larmor radius effects, but an energetic tail forms since the energy per resonating particle is large for the minority species. ^3He minority heating may be a good choice during the start-up phase of a burning plasma but may be disadvantageous when the fusion alphas provide a large part of the heating as the ^3He dilutes the fuel. However, if minority heating is applied, the ^3He population will also be confined and therefore its concentration in the burning plasma may not drop very fast, leaving a small population of ^3He . Moreover, radioactive decay of tritium leads to a ^3He nucleus, and hence deuterium-tritium plasmas will always contain at least trace amounts of ^3He . We investigate here ^3He concentrations of 1% – 4% in 1% steps and also calculate a scenario with 0.1% ^3He concentration.

The simulations indicate that the CTS signal fraction of ^3He as a function of ^3He concentration has a maximum in each case: 3% for 20 MW and 4% or more for 40 MW ICRH power. An optimum concentration exists due to the fact that a very low ^3He concentration obviously results in a small fast ion population whereas a very high concentration leads to a lower power per resonating particle. The maximum for minority heating with ^3He concentration of 4% and 40 MW ICRH power lies at $R = 6.76$ m and $Z = 0.76$ m.

The scattering functions for 3% ^3He with 20 MW is revealed in Figure 4. It becomes clear that the ^3He for minority heating produces a stronger signal contribution than the tritium does for pure tritium heating. Contrary to the former case, the ^3He feature reaches up to 10–20% of the alpha feature even for the nominal ICRH power of 20 MW. The triton CTS signal component always falls clearly short of the fusion alpha CTS signal component by more than an order of magnitude in minority heating scenarios. The reason for the strong CTS signal component lies partly in the power deposition profiles and partly in the dependence of the CTS signal on the square of the charge of the ion species as mentioned in section 4.1. The scattering volume with the maximum CTS signal contribution lies slightly towards the HFS for ^3He compared to tritium. The fundamental resonance of ^3He coincides with the second harmonic resonance of tritium. However, in the minority heating scheme, the E_+ component

of the wave electric field (the component rotating in the Larmor direction of the resonating ions) is the primary source of the acceleration of the minority species. The E_+ component peaks on the HFS of the cyclotron resonance, and ions seeing a Doppler broadened resonance on the HFS therefore have the strongest absorption. Contrarily, in the case of majority second harmonic heating, the E_+ component does not have the same tendency. Thus, the ^3He cases have a maximum power absorption shifted towards the HFS as compared to pure second harmonic tritium heating. The absorbed power density is therefore larger. It becomes clear that only the minority species ^3He can produce a CTS signal contribution on the same order as the fusion alphas for ICRH, although it is still smaller and very localized.

The sensitivities of the power deposition profiles to the ^3He concentration and the ICRH power levels are displayed in Figures 6(a) and 6(b) for 20 and 40MW, respectively. The results depend rather strongly on the ^3He concentration since the polarization of the wave and the absorption strength both change with ^3He concentration. For these low ^3He concentrations, the wave damping increases with concentration. Strong wave damping, occurring for large concentrations, leads to a very peaked deposition profile whereas lower damping leads to a less peaked deposition profile. The polarization affects the location of maximum power deposition, such that the power is deposited further towards the HFS for larger minority species concentrations. The volumetric effect then additionally leads to the larger power densities.

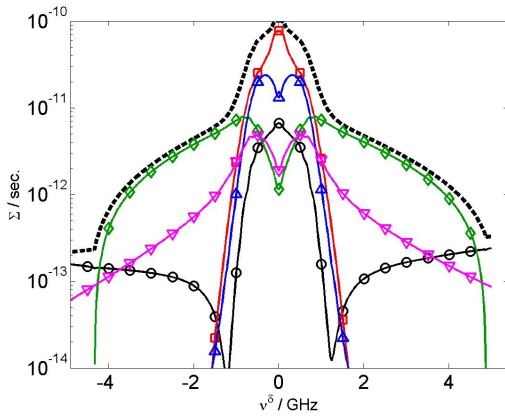


FIG. 4. Scattering function 3% ^3He concentration and 20 MW heating power; $R = 6.76$ m, $Z = 0.76$ m, $\varphi = 101^\circ$, $\theta = 157^\circ$; \blacklozenge -alphas, \blacktriangle -tritons, \blacktriangledown - ^3He , \blacksquare -bulk ions, \bullet - electrons, - - - total

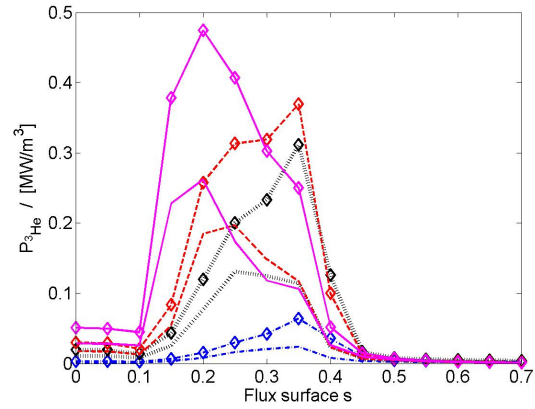


FIG. 5. Power deposition profiles on ^3He for various ^3He concentrations and heating powers; curves with symbols – 40 MW, curves without symbols – 20 MW; concentrations: — 4%, - - - 2%, \cdots 1%, - · - 0.1%

5. Conclusions

The fast ion CTS diagnostic will enable inferences about the fusion alpha distributions even in the presence of energetic ions due to off-axis ICRH in ITER. The triton CTS signal component is always at least an order of magnitude below the alpha CTS signal component, even in a scenario with an upgraded heating power of 40 MW. However, the strongest CTS signal contribution from ICRH is expected for a ^3He minority heating scheme. In a particular limited region, the contribution of the fast ^3He can be larger than $\sim 10\%$ of the alpha feature, making it difficult to draw conclusions about the alpha particles for resolution of near

perpendicular velocities. Outside this region with a width of ~20–30 cm, the results indicate that the CTS diagnostic will allow conclusions about physics of fast alpha particles.

Acknowledgments

This work, supported by the European Communities under the contract of Association between EURATOM / Risø DTU, was partly carried out within the framework of the European Fusion Development Agreement. The views and opinions expressed herein do not necessarily reflect those of the European Commission.

References

- [1] Jacquinot *et al.* 1999 Nucl. Fusion **39** 2471–2495
- [2] Fasoli *et al.* 2007 Nucl. Fusion **47** S264 – S284
- [3] Chen and Zonca 2007 Nucl. Fusion **47** S727 – S734
- [4] Heidbrink and Sadler 1994 Nucl. Fusion **34** 535
- [5] Heidbrink W 2002 Phys. Plasma **9** 2213 – 2219
- [6] Rosenbluth and Rutherford 1975 Phys. Rev. Lett. **34** 1428–1431
- [7] Cheng and Chance 1986 Phys. Fluids **29** 3695–3701
- [8] Wong 1999 Plasma Phys. Control. Fusion **41** R1–R56
- [9] Zweben *et al.* 2000 Nucl. Fusion **40** 91 – 149
- [10] Pinches *et al.* 2004 Plasma Phys. Control. Fusion **46** B187–B200
- [11] Chen 1994 Phys. Plasma **1** 1519–1522
- [12] Briguglio *et al.* 2007 Phys. Plasma **14** 055904–055904–10
- [13] Günter *et al.* 2007 Nucl. Fusion **47** 920–928
- [14] Bindslev *et al.* 1999 Phys. Rev. Lett. **83**(16) 3206–3209
- [15] Bindslev *et al.* 2006 Phys. Rev. Lett. **97** 205005–1–2005005–4
- [16] Bindslev *et al.* Plasma Phys. Control. Fusion **49** B551–B562
- [17] Nielsen *et al.* 2008 Phys. Rev. E **77** 16407
- [18] Bindslev 1993 Plasma Phys. Control. Fusion **35**(11) 1615–1640
- [19] Bindslev 1996 J. Atmos. Terr. Phys. **58** 983
- [20] Egedal *et al.* 2005 Nucl. Fusion **45** 191–200
- [21] Salewski *et al.* 2008 submitted
- [22] Eriksson *et al.* 1993 Nucl. Fusion **33** 1037–48
- [23] Eriksson and Hellsten 1995 Phys. Scripta **53** 70
- [24] Donne *et al.* 2007 Nucl. Fusion **47** S337 – S384
- [25] Bindslev *et al.* 2004 Rev. Sci. Instrum. **75**(10) 3598–3600
- [26] Meo F *et al.* 2004 Rev. Sci. Instrum. **75** 3585–3588
- [27] Tsakadze *et al.* 2008 Fusion Sci. Tech. **53** 69 –76
- [28] Shimada *et al.* 2007 Nucl. Fusion **47** S1–S17
- [29] Polevoi 2002 J. Plasma Fusion Res. SERIES **5** 82
- [30] Chang 1985 Phys. Fluids **28** 3598
- [31] Bergeaud *et al.* 2000 Nucl. Fusion **40** 35–51